

Theoretical Analysis of a Rayleigh-Raman Polychromatic Laser Guide Star

Lennon O. Reinhart^a, Michael Hart^a, and Yushi Kaneda^a

^aCollege of Optical Sciences, University of Arizona, 1630 E University Blvd, Tucson, AZ, USA

ABSTRACT

Wavefront tilt correction is extremely important in the adaptive optics systems of large astronomical telescopes, for tilt makes up most of the aberration induced by atmospheric turbulence. Tilt measurement methods typically used in adaptive optics systems today involve light from a natural guide star in the vicinity of the object of interest, or from the object itself. A typical laser guide star does not allow for tilt measurement due to the double-pass nature of the reference light; the deflection of the upward traveling reference light is unknown. Polychromatic laser guide stars allow for object-independent tilt measurement by utilizing the dispersion of the refractive index of air and differential tilt measurements at different wavelengths. Existing research has been focused on polychromatic sodium laser guide stars (PSLGS), while Rayleigh-Raman polychromatic laser guide stars (RRPLGS) have seemingly been overlooked. It is shown that RRPLGS have a number of advantages, including scalability of returned flux and flexibility in selection of short wavelengths, allowing for a combination of multiple tilt measurements. RRPLGS are applicable to all sizes of telescopes, keeping in mind that for large telescopes the cone effect is minimized by assuming a tomographic wavefront sensing system. A theoretical analysis of a specific RRPLGS system is presented to address the feasibility of RRPLGS, focusing on fundamental constraints.

1. INTRODUCTION

Tilt is a significant portion of the aberrations caused by atmospheric turbulence. Specifically, two-axis tilt makes up roughly 87% of the phase variance of the aberration induced by Kolmogorov turbulence. Existing tilt measurement systems require light from a source that traverses the medium in single pass as a tilt measurement reference, such as a natural guide star or the object itself. Laser guide stars (LGS) create a reference source in the field of view to enable a wavefront measurement through turbulence. However, typical existing LGS cannot act as a tilt measurement reference source due to the fundamental problem of the double pass nature of the reference light. In other words, the deflection of the upward traveling reference light is unknown.

Polychromatic laser guide stars (PLGS) can enable tilt correction that is independent of the object being viewed and natural guide stars. PLGS rely on atmospheric dispersion and the assumption that the multiple wavelengths from the guide star come from the same point in space. Existing research on PLGS has focused on polychromatic sodium LGS (PSLGS), while Rayleigh-Raman polychromatic LGS (RRPLGS) seem to have been overlooked. This paper investigates the unique benefits of RRPLGS through analytical equations and numerical simulation.

2. OVERVIEW

From the dispersion of the refractive index of air and the separability of wavelength and atmospheric characteristics (e.g. temperature, pressure), the general relationship,

$$\theta = \Delta\theta \frac{(n-1)}{\Delta n}, \quad (1)$$

is derived.¹ All PLGS use this relationship. In Equation (1), θ is any quantity derived from a linear operation on the wavefront that the imaging system is sensitive to, $\Delta\theta$ is the difference between two measurements of θ at two separate wavelengths, n is the refractive index at the wavelength of observation, and Δn is the difference between the refractive index at the same wavelengths as those in $\Delta\theta$. The proportionality in Equation (1) assumes that

the light of different wavelengths is reaches a point of observation from paths that are not significantly different from each other.

From this fundamental relationship, RRPLGS is realized as a technique that can be successfully implemented. RRPLGS depends on Rayleigh and Raman scattering in the atmosphere from N_2 and O_2 molecules and therefore is scalable in the magnitude of the backscattered light. In other words, there is no limit on the laser power. Like conventional Rayleigh scattering LGS, the laser used needs to be pulsed to permit range gating but otherwise does not need to be specialized, i.e. does not need to be tuned to a specific wavelength and polarization corresponding to a specific energy transition. For any single laser, there are various Raman backscattering mechanisms that can potentially be leveraged to yield multiple tilt measurements at the wavelength of observation. These multiple tilt measurements from a single laser can be combined for an improved tilt measurement. See Sections 4 and 5 for details regarding combination of measurements and Raman processes.

Furthermore, multiple different wavelength lasers can be used to yield multiple tilt measurements because Rayleigh and Raman scattering do not require a specific excitation wavelength. Because the returned photon flux from both Rayleigh and Raman scattering is inversely proportional to the laser wavelength to the fourth power, there is a range of laser wavelengths that is practical. This continuous wavelength range has a lower bound due to the absorption of ozone in the near UV and an upper bound due to the magnitude of returned flux from Raman scattering.

While there are many advantages to RRPLGS, there are a number of disadvantages that seem to have been the reasoning for the scientific community to focus efforts on PSLGS.¹ Just as with conventional Rayleigh scattering LGS, the RRPLGS will be limited to an altitude of no more than about 30 km.² Nevertheless, most turbulence is below 20 km – namely, at ground level and at 10 km.³ Raman scattering cross sections of N_2 and O_2 are considerably small, resulting in low return flux relative to the Rayleigh line. Another disadvantage is that Raman scattering is usually limited in the spectral separation of any two wavelengths used in the returned spectra (from a single laser) to yield a differential tip-tilt measurement, which is related to limitation in Δn . Equation (1) above implies that a large Δn is desired for an accurate tilt measurement.

3. PRINCIPLES OF OPERATION

For combinations of tilt measurements made with a single laser, the notation is such that λ_o is the wavelength of observation, i is the i^{th} measurement of the tilt at λ_o from a single laser, and w indicates the first or second wavelength corresponding to this i^{th} measurement and can only equal 1 or 2. This tilt measurement is associated with the laser number, L , which is always a positive integer and is the L^{th} measurement of the tilt at λ_o related to the use of multiple lasers. For each i^{th} measurement, there is a pair of wavelengths used that must be clearly identified. Thus, the wavelengths in this pair will be denoted by $\lambda_{L,w,i}$. This notation is important for combinations of tilt measurements made with multiple lasers. Note that $\lambda_{L,w,i}$ corresponds to light that is traveling towards the imaging system. Figure 1 shows an example layout.

From Equation (1) above, it can be stated that

$$\sigma_{est,L,i}^2 = \sigma_{diff,L,i}^2 \left(\frac{n(\lambda_o) - 1}{n(\lambda_{L,1,i}) - n(\lambda_{L,2,i})} \right)^2, \quad (2)$$

where for the L^{th} laser, $\sigma_{est,L,i}^2$ is the variance in the i^{th} measurement of the tilt at the wavelength of observation. In other words, $\sigma_{est,L,i}$ is the tilt measurement uncertainty in units of radians of wavefront angle. $\sigma_{diff,L,i}^2$ is the variance in the i^{th} measurement of the differential tilt. The measured differential tilt is simply the difference between the measured tilt at $\lambda_{L,1,i}$ and the measured tilt at $\lambda_{L,2,i}$.

Assuming the two tilt measurements that are differenced are independent relative to each other (as is done in Schöck et al.⁴). It follows that

$$\sigma_{diff,L,i}^2 = \sigma_{L,1,i}^2 + \sigma_{L,2,i}^2, \quad (3)$$

where $\sigma_{L,w,i}$ is the uncertainty in the measurement of the tilt using $\lambda_{L,w,i}$. Note that $\sigma_{L,w,i}$ takes into account both the temporal and spatial uncertainty.

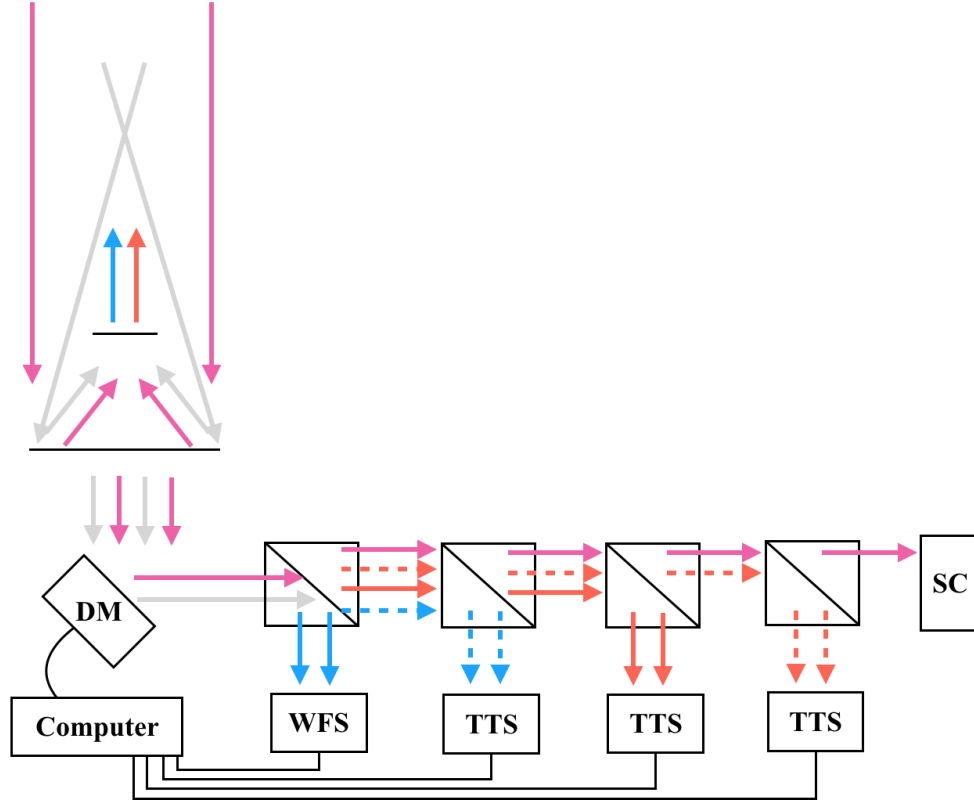


Figure 1. Example RRPLGS system layout assuming two lasers are used and only two of the returned wavelengths are used per laser (thus in this case i is always equal to 1), one of which is the Rayleigh line. In this case the two Rayleigh wavelengths are represented by the solid red ($\lambda_{1,1,1}$) and blue ($\lambda_{2,1,1}$) lines, and the counterpart dotted red ($\lambda_{1,2,1}$) and blue ($\lambda_{2,2,1}$) lines represent Raman wavelengths. The purple line represents the science wavelength, λ_o . The gray line is a shorthand for the solid red and blue and dotted red and blue lines. DM stands for deformable mirror, WFS for wavefront sensor, TTS for tip-tilt sensor, and SC for science camera. Beam splitters are used as an example to separate the spectrum.

$\sigma_{L,w,i}$ is related to $\sigma_\alpha(\lambda_{L,w,i})$, the angular position measurement uncertainty for a plane tilted wavefront, by an average of the tilts measured over a number of subapertures (Zernike tip-tilt is the least-mean-square slope of the wavefront). Thus

$$\sigma_{L,1,i} = \frac{\sigma_\alpha(\lambda_{L,w,i})}{\sqrt{g_{L,w,i}}}, \quad (4)$$

in which $g_{L,w,i}$, the number of subapertures in the entrance pupil, is approximated by an object-space area ratio

$$g_{L,w,i} = \frac{D_r^2}{d_{L,w,i}^2}, \quad (5)$$

where D_r is the diameter of the entrance pupil of the receiving telescope and $d_{L,w,i}$ is the subaperture size. Note that different wavelengths (designated by L , w , and i) can be directed to different wavefront sensors. In the case of a tip-tilt sensor, a single lens (as opposed to a lenslet array) is used to sense the overall wavefront tip and tilt across the entire pupil, i.e. sense the global tip and tilt. This can be thought of as a Shack-Hartmann wavefront sensor (SHWFS) with one ‘‘subaperture.’’ In such a case, $d_{L,w,i}$ is the size of a single lens that has the same object space size as the entrance pupil diameter, making $g_{L,w,i}$ equal unity.

$\sigma_\alpha(\lambda_{L,w,i})$ for a SHWFS is derived by Hardy³ and is taken in this context as the tip-tilt measurement

uncertainty corresponding to the wavelength $\lambda_{L,w,i}$,

$$\sigma_\alpha(\lambda_{L,w,i}) = \frac{\sqrt{2}\pi}{8SNR_{L,w,i}} \left[\left(\frac{3\lambda_{L,w,i}}{2r_o(\lambda_{L,w,i})} \right)^2 + \Delta\alpha^2 \right]^{1/2} \quad r_o(\lambda_{L,w,i}) < d_{L,w,i}. \quad (6)$$

In the equation above, $\Delta\alpha$ is the object space subtense of the beacon in radians of angle. $\Delta\alpha$ is described in more detail below. $r_o(\lambda_{L,w,i})$ is the Fried length and is a function of wavelength. $SNR_{L,w,i}$ is defined in Equation (7) and is the signal to noise ratio corresponding to the w^{th} wavelength related to the i^{th} measurement for the L^{th} laser. Assuming random perturbations, the tilt in two orthogonal directions is taken into account by multiplying by $\sqrt{2}$, as shown in Equation (6). If the size of the subaperture in object space is more limiting than the Fried length, i.e. if $d_{L,w,i}$ is less than $r_o(\lambda_{L,w,i})$, then $r_o(\lambda_{L,w,i})$ in Equation (6) is replaced by $d_{L,w,i}$. To convert the units of $\sigma_\alpha(\lambda_{L,w,i})$ from radians of wavefront angle to radians of phase error, Equation (6) is multiplied by $2\pi d/\lambda_{L,w,i}$.

The signal to noise ratio (corresponding to the wavelength $\lambda_{L,w,i}$) for a unity gain quad-cell detector with negligible detected background electrons per pixel is given by Hardy³ as

$$SNR_{L,w,i} = \frac{n_p(\lambda_{L,w,i})}{(n_p(\lambda_{L,w,i}) + p_s e^2)^{1/2}}, \quad (7)$$

where p_s is the number of pixels per subaperture, e is the read noise per pixel in units of electrons rms, and n_p is the expected number of photons per measurement per subaperture. The equation for n_p is also given by Hardy,³

$$n_p(\lambda_{L,w,i}) = M_{L,w,i} \left[\frac{\lambda_{L,w,i} \sigma_{B,L,w,i} N(z)_{L,w,i} \Delta z T_{A,L,w,i} T_{A,A}}{hc \cdot 4\pi \cdot z^2} \right] E_{L,w,i} T_L T_o A_{L,w,i}. \quad (8)$$

The transmission factors are given by $T_{A,L,w,i}$, $T_{A,A}$, T_L , and T_o , and are the one-way transmission of atmosphere between the telescope and the beacon corresponding to the wavelength $\lambda_{L,w,i}$, the one-way transmission of atmosphere between the telescope and the beacon corresponding to the laser light traveling away from the imaging system (not necessarily equal to $\lambda_{L,w,i}$), the transmission of the laser path to the projection aperture, and the transmission of optical components in the transmit and receive paths, respectively. Notice that if the wavelength is the same in transmission and reception then $T_{A,A} = T_{A,L,w,i}$. $M_{L,w,i}$ is the number of laser pulses received within the integration time corresponding to a tip-tilt or higher-order measurement; note that $M_{L,w,i}$ is further specified as per tip-tilt measurement ($M_{TT,L,w,i}$) or per higher-order measurement ($M_{HO,L,w,i}$). The distance from the telescope to the center of the range gate is z , in meters. The effective backscatter cross section in m^2 corresponding to the wavelength $\lambda_{L,w,i}$ is given by $\sigma_{B,L,w,i}$. The atmospheric density of the scattering molecules as a function of z , the range to the center of the range gate, is given by $N(z)_{L,w,i}$ in units of m^{-3} . $E_{L,w,i}$ is the laser energy per pulse in Joules corresponding to the wavelength $\lambda_{L,w,i}$. The area of the receiving aperture (or subaperture) is $A_{L,w,i}$, h is the Planck constant, and c is the velocity of light. Δz is the chosen receiver range gate length in units of meters. As discussed by Thompson and Gardner,⁵ the maximum allowable receiver range gate length is $\Delta z_{max}(\lambda_{L,w,i})$ and corresponds to the diameter of the laser guide star matched to the natural stellar width, $\Delta\alpha_{star}(\lambda_{L,w,i})$. This maximum allowable receiver range gate length is found geometrically to be

$$\Delta z_{max}(\lambda_{L,w,i}) = \frac{2D_e \Delta\alpha_{star}(\lambda_{L,w,i}) z^2}{D_e^2 - (z \Delta\alpha_{star}(\lambda_{L,w,i}))^2}, \quad (9)$$

where

$$\Delta\alpha_{star} = \frac{\lambda_{L,w,i}}{r_o(\lambda_{L,w,i})} \quad r_o(\lambda_{L,w,i}) < d_{L,w,i}. \quad (10)$$

Note that D_e , the diameter of the laser emission telescope aperture, does not have to be the full aperture of the telescope. In fact, Thompson and Gardner show that D_e should be chosen to be as small as possible, but large enough for a reasonably stable LGS centroid.⁵ Typically a value of approximately $3r_o(\lambda_{L,w,i})$ is chosen for D_e . Rearranging Equation (9), an expression relating an arbitrary range gate length Δz and the corresponding angular size of the beacon, $\Delta\alpha$, is

$$\Delta\alpha = \frac{D_e}{z \Delta z} \left(-z + \sqrt{z^2 + \Delta z^2} \right). \quad (11)$$

Δz will ultimately be chosen to minimize the the total wavefront error budget, but for the purposes of this preliminary analysis it will be chosen based on spot elongation. The elongation angle describing angular extent of the range gate, i.e. elongated beacon, as seen from a transverse distance of r from the center of the entrance pupil is given via simple geometry and small angle approximation by

$$\theta_{elong} = \frac{r\Delta z}{z^2 - \left(\frac{\Delta z}{2}\right)^2}. \quad (12)$$

Letting the approximate LGS FWHM be the average wavelength over the Fried length, the total angular extent of the spot in the radial direction is approximated by adding in quadrature. Defining θ_{total} as the seeing limit multiplied by a fraction Q ,

$$\theta_{total} = \sqrt{\left(\frac{\lambda_{avg}}{r_o(\lambda_{avg})}\right)^2 + \theta_{elong}^2} = Q \frac{\lambda_{avg}}{r_o(\lambda_{avg})}. \quad (13)$$

Notice that Q must be greater than 1. Approximating Δz as small such that the denominator in Equation (12) is simplified, the approximate Δz corresponding to a value for Q is

$$\Delta z = \frac{\lambda_{avg} z^2}{r_o(\lambda_{avg}) r} \sqrt{Q^2 - 1}. \quad (14)$$

As for the choice of $M_{L,w,i}$, the system is limited by $\tau_{c,L,w,i}$, the coherence time (for wavelength $\lambda_{L,w,i}$). However, $\tau_{c,L,w,i}$ is a summary statistic that describes the change in the entire wavefront, not a particular mode (e.g. tilt), so it is very conservative for changes in tilt, for tilt is more slowly varying. Tyler has investigated the fundamental tracking frequency for the Zernike tip and tilt and shown that this correction frequency is approximately one ninth of the Greenwood frequency,⁶ i.e.

$$f_{z,L,w,i} = \frac{1}{9} f_{G,L,w,i} = \frac{1}{9} \frac{0.134}{\tau_{c,L,w,i}} = \frac{1}{9} \frac{0.134v}{0.314r_o(\lambda_{L,w,i})}. \quad (15)$$

v is the wind velocity at the altitude of correction. The number of laser pulses per tip-tilt measurement is then given by $f_{z,L,w,i}$ divided by the laser pulse repetition rate, $f_{p,L}$,

$$M_{TT,L,w,i} = \frac{f_{p,L}}{f_{z,L,w,i}}. \quad (16)$$

Likewise, the number of laser pulses per higher-order measurement is given by

$$M_{HO,L,w,i} = \frac{f_{p,L}}{f_{G,L,w,i}}. \quad (17)$$

Equations (2)-(8) and (11) are used to form an expression for $\sigma_{est,L,i}^2$. In the shot noise limit, i.e. when $SNR_{L,w,i}$ is simplified to be $\sqrt{n_p(\lambda_{L,w,i})}$, this expression is

$$\sigma_{est,L,i}^2 = \left(\frac{\sqrt{2}\pi}{8}\right)^2 (Y_{L,1,i} + Y_{L,2,i}) \left(\frac{n(\lambda_o) - 1}{n(\lambda_{L,1,i}) - n(\lambda_{L,2,i})}\right)^2, \quad (18)$$

where

$$Y_{L,w,i} = \frac{4\pi h c z^2 \left[\left(\frac{3\lambda_{L,w,i}}{2r_o(\lambda_{L,w,i})}\right)^2 + \left(\frac{D_e}{z\Delta z}(-z + \sqrt{z^2 + \Delta z^2})\right)^2 \right]}{g_{L,w,i} M_{L,w,i} \lambda_{L,w,i} \sigma_{B,L,w,i} N(z)_{L,w,i} \Delta z T_{A,L,w,i} T_{A,A} E_{L,w,i} T_L T_o A_{L,w,i}}. \quad (19)$$

4. COMBINATIONS OF MEASUREMENTS

The optimal combination of the various tip-tilt measurements at the wavelength of observation is of particular interest. This can yield a reduced variance in the final measurement. It is required that each different wavelength laser results in two or more wavelengths returning towards the imaging system. One way to improve the accuracy of the tip-tilt measurement at the wavelength of observation is to combine the measurements arising from all pairs of wavelengths in the spectrum of the returned light. This makes the most out of each laser. Additionally, with many different wavelength lasers, the tip-tilt measurement at the wavelength of observation from each different wavelength laser can be combined. In other words, the combinations possible are twofold; there are combinations related to the use of one laser, and there are combinations related to the use of multiple lasers. Note that in calculating any single tip-tilt estimate at the wavelength of observation, the pair of wavelengths used must come from the result of one laser. This is because the wavelength pairs used for a differential tilt measurement must be known to have come from the same point in space. The returned light from a laser of one wavelength and the returned light from a laser of another wavelength are not known to have come from the same point in space because the deflection of the reference light traveling towards the object of observation is unknown.

4.1 Combinations Related to Multiple Lasers

The combinations related to the use of multiple lasers are discussed first. Once a tip-tilt measurement at the wavelength of observation is found from a single laser, whether it be from a single pair of wavelengths or a combination of pairs of wavelengths from the returned light spectrum, this result can be combined with that of additional lasers of different wavelength via a weighted average. Each measurement is optimally weighted by the reciprocal square of the associated uncertainty via maximum likelihood. The tip-tilt measurement at the wavelength of observation for each different wavelength laser is identified by laser number L (the maximum value of L is L_{max} , the number of different wavelength lasers used), and has an uncertainty of $\sigma_{best,Las,L}$. The best estimate for the mean of the true tilt is given by

$$\theta_{best,final} = \frac{\sum_{L=1}^{L_{max}} \frac{\theta_{best,Las,L}}{\sigma_{best,Las,L}^2}}{\sum_{L=1}^{L_{max}} \frac{1}{\sigma_{best,Las,L}^2}}. \quad (20)$$

$\theta_{best,Las,L}$ is defined in Equation (22). Assuming that the tip-tilt measurements of the wavelength of observation from different lasers are uncorrelated, $\sigma_{best,final}$, the uncertainty in the weighted average of the tilt measurements from different lasers, can be calculated via error propagation,

$$\sigma_{best,final} = \left(\sum_{L=1}^{L_{max}} \frac{1}{\sigma_{best,Las,L}^2} \right)^{-1/2}. \quad (21)$$

Note that if only one measurement of the tilt at the wavelength of observation is found per laser (i.e. the maximum value of i is unity), then $\sigma_{best,Las,L}^2$ simply equals $\sigma_{est,L,1}^2$. As for the combinations related to the use of one laser, one cannot safely assume that the tip-tilt measurements at the wavelength of observation are uncorrelated. The following relates $\sigma_{est,L,i}^2$ to $\sigma_{best,Las,L}^2$ for multiple single-laser measurements of the tilt (the maximum value of i is greater than 1) at the wavelength of observation.

4.2 Combinations Related to a Single Laser

In the context of combinations related to the use of one laser (L is fixed), let $\theta_{est,L,i}$ be the i^{th} measurement of the tilt at the wavelength of observation (using the L^{th} laser) with measurement uncertainty $\sigma_{est,L,i}$. $\vec{\theta}_{est}$ is a real and random vector of various $\theta_{est,L,i}$ and has dimensions $q \times 1$. Let q be the number of pairs of returned wavelengths from a single laser (the maximum value of i is q). Assuming that $\vec{\theta}_{est}$ is normally distributed, i.e. the probability density function of $\vec{\theta}_{est}$ given the mean θ is a q -dimensional normal of mean θ and covariance matrix \mathbf{K}_θ , the method of maximum likelihood yields that when using only one laser, the best estimate of the mean of the true tilt is given by

$$\theta_{best,Las,L} = \frac{\vec{\theta}_{est}^T \mathbf{K}_\theta^{-1} \vec{\xi}}{\vec{\xi}^T \mathbf{K}_\theta^{-1} \vec{\xi}}, \quad (22)$$

where $\vec{\xi}$ is a $q \times 1$ column vector of ones. It is easy to show that given the general form $\vec{y} = \mathbf{B}\vec{x}$, the covariance matrix of \vec{y} , \mathbf{K}_y , is related to that of \vec{x} by is $\mathbf{K}_y = \mathbf{B}\mathbf{K}_x\mathbf{B}^T$. Likewise $\vec{y} = \beta\mathbf{B}\vec{x}$, yields $\mathbf{K}_y = \beta^2\mathbf{B}\mathbf{K}_x\mathbf{B}^T$, where β is a scalar. This can further be extended by stating a general form $y = \beta\vec{\xi}^T\mathbf{B}\vec{x}$, which yields that the variance of y is $\sigma_y^2 = \beta^2\vec{\xi}^T\mathbf{B}\mathbf{K}_x\mathbf{B}^T\vec{\xi}$. Applying this general form to Equation (22) and noting that covariance matrices are Hermitian, i.e. $\vec{\theta}_{est}^T\mathbf{K}_\theta^{-1}\vec{\xi} = \vec{\xi}^T\mathbf{K}_\theta^{-1}\vec{\theta}_{est}$ for this real case, yields that when using only one laser the uncertainty of the best estimate of the mean of the true tilt is given by

$$\sigma_{best,Las,L} = \left(\vec{\xi}^T \mathbf{K}_\theta^{-1} \vec{\xi} \right)^{-1/2}. \quad (23)$$

Note that if the elements of $\vec{\theta}_{est}$ are not correlated, Equation (23) matches the form of Equation (21) and Equation (22) is reduced to an optimally weighted average akin to Equation (20).

5. RAMAN SCATTERING PROCESSES OF INTEREST

Combinations related to the use of multiple lasers can be realized simply considering one Raman process, but the combinations related to the use of one laser are made possible by taking into account multiple Raman scattering processes. Rayleigh scattering (elastic) off air molecules provides the largest signal, which can be used for high-order wavefront sensing. Raman scattering (inelastic) results in weaker signals that are Raman shifted to wavelengths that differ from the laser wavelength. At altitudes less than 100 km, the composition of air is approximately 76% N₂ and 21% O₂.

The Raman scattering processes of interest to investigate include vibrational (Stokes and Anti-Stokes), rotational, stimulated, and cascaded. Vibrational Q-branch transitions result in a shift in wavelength characterized by the Raman shift (2331 cm⁻¹ for N₂ and 1555 cm⁻¹ for O₂), and the cross section as a function of wavelength is given by Bischel and Black.⁷ A Raman shift that results in a longer wavelength (Stokes) is more common and thus has more flux than a Raman shift that results in a shorter wavelength (Anti-Stokes). The spectra associated with rotational Raman scattering is observed surrounding the Rayleigh line and the vibrational Raman lines. Rotational Raman shifts range from approximately 5 cm⁻¹ to 200 cm⁻¹ from the central line⁸ and have lower flux than vibrational Raman scattering. The rotational Raman cross section as a function of wavelength for N₂ and O₂ are given by Penney et al.⁹ Stimulated Raman scattering uses two (in this case, co-linear in space) lasers with the same polarization that have a difference in wavelength equal to a wavelength corresponding to a Raman transition (with a characteristic Raman shift) of the molecule. It is the difference in wavelength between the two lasers that matters in this case. Stimulated Raman scattering results in Raman scattered light that is several orders of magnitude brighter than typical (spontaneous) Raman scattering. Cascaded Raman scattering occurs with high laser pulse energy and results in multiple orders of Raman scattering, i.e. a larger separation of wavelength from the Rayleigh line. This is of particular interest in RRPLGS because a high laser power is possible with RRPLGS and a large Δn is beneficial (see Equations (1) and (2)).

6. SIMULATION

Using the equations above, a specific system model is simulated with the parameters in Table 1. For this preliminary simulation, only Rayleigh scattering and Stokes vibrational Q-branch Raman scattering from N₂ is taken into account. In other words, only one measurement of the tilt at λ_o is found per laser, and combinations related to the use of one laser are not included. Note that data from Chapter 7 of the *Handbook of Geophysics and Space Environments*¹⁰ is used for atmospheric transmission as a function of wavelength ($T_{A,A}$ and $T_{A,L,w,i}$) with observation angle at zenith. Pressure and temperature values used for Rayleigh cross section and atmospheric density of N₂ as a function of altitude have been sourced from Allen.¹¹

To compare the SNR between various spectral lines, the SNR taking into account the entire collecting area (called the tilt SNR) is plotted against the returned wavelength spectrum in Figure 2. In the shot noise limit, the SNR taking into account the entire collecting area is given by $SNR_{L,w,i}$ multiplied by $\sqrt{g_{L,w,i}}$, since n_p is multiplied by $g_{L,w,i}$ to take into account the entire collecting area. Notice that the 361 nm returned wavelength is sent to the SHWFS for higher-order mode correction, and because $M_{HO,L,w,i} < M_{TT,L,w,i}$ the SNR is lower.

Table 1. Key input parameters of specific system model simulation.

System Parameter	Symbol	Units	Value
Wavelength of Observation	λ_o	nm	1500
Object Space Tip-Tilt Aperture Size and Telescope Diameter	D_r	m	3
Rayleigh Wavelength Corresponding to Laser 1 (Nd:YLF)	$\lambda_{1,1,1}$	nm	349
Rayleigh Wavelength Corresponding to Laser 2 (Nd:YAG)	$\lambda_{2,1,1}$	nm	355
Rayleigh Wavelength Corresponding to Laser 3 (Nd:YAIO)	$\lambda_{3,1,1}$	nm	361
Laser Energy Per Pulse (For All Lasers)	E	mJ	40
Laser Pulse Repetition Rate	f_p	kHz	5
Number of Pulses Captured Per Tip-Tilt Measurement	$M_{TT,L,w,i}$	pulses	300
Number of Pulses Captured Per Higher-Order Measurement	$M_{HO,L,w,i}$	pulses	33
Range to Center of Range Gate	z	km	12
Range Gate Length	Δz	km	0.6
Laser Emission Telescope Diameter	D_e	cm	30
Fried Length at 500 nm	$r_o(500 \text{ nm})$	cm	15

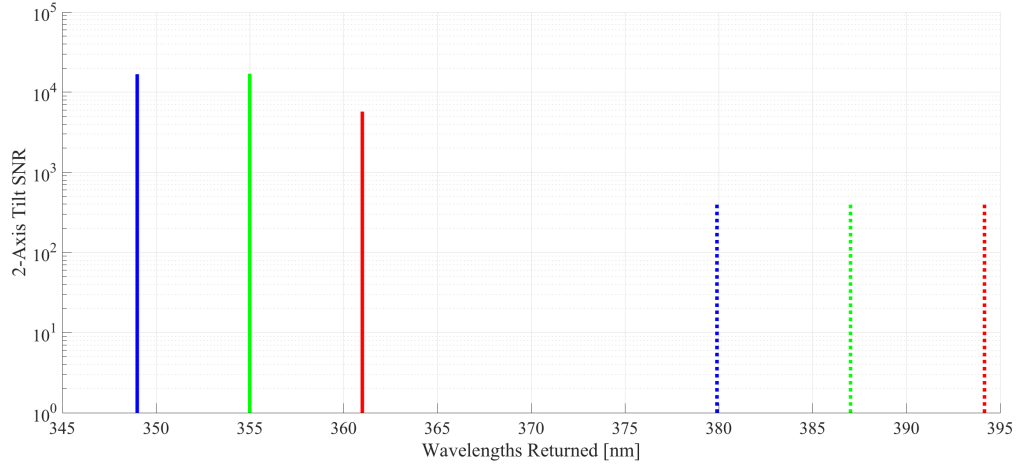


Figure 2. 2-axis tilt SNR as a function of returned wavelength. The Rayleigh wavelengths are represented by the solid lines while the counterpart dotted lines correspond Raman lines. The lines of the same color represent a pair of wavelengths used to measure the tilt at the wavelength of observation.

As expected, due to the small Raman cross section, the SNR of Raman lines is relatively low compared to the Rayleigh. The high laser power results in high SNR values.

To compare the effectiveness of each laser in reducing the uncertainty in the weighted average (see Equation (21)), $\sigma_{best,Las,L}$ for $L = 1, 2$, and 3 are compared in Table 2. The uncertainties are extremely similar. This is due to the impact of $g_{L,w,i}$ in Equation (4) and the refractive index term in Equation (2) increasing with longer laser wavelength due to the Raman shift (2331 cm^{-1}). Applying Equation (21), the resulting uncertainty in the weighted average, $\sigma_{best,final}$, is 0.12 arcsec of wavefront angle. For reference, the diffraction limit λ_o/D_r is 0.10 arcsec of wavefront angle.

Keeping all system parameters the same but now using only one laser, the tilt measurement uncertainty corresponding to one laser can be analyzed as a function of wavelength and laser power. Note that for this single

Table 2. Comparison of the tilt measurement uncertainty (in units of arcseconds of wavefront angle) as function of laser wavelength. The resulting uncertainty in the weighted average is 0.12 arcsec of wavefront angle.

Laser Wavelength [nm]	Two-Axis Tilt Measurement Uncertainty [Arcsec]
349	0.201
355	0.204
361	0.207

laser case, high-order mode correction is included by directing the Rayleigh line to a SHWFS.

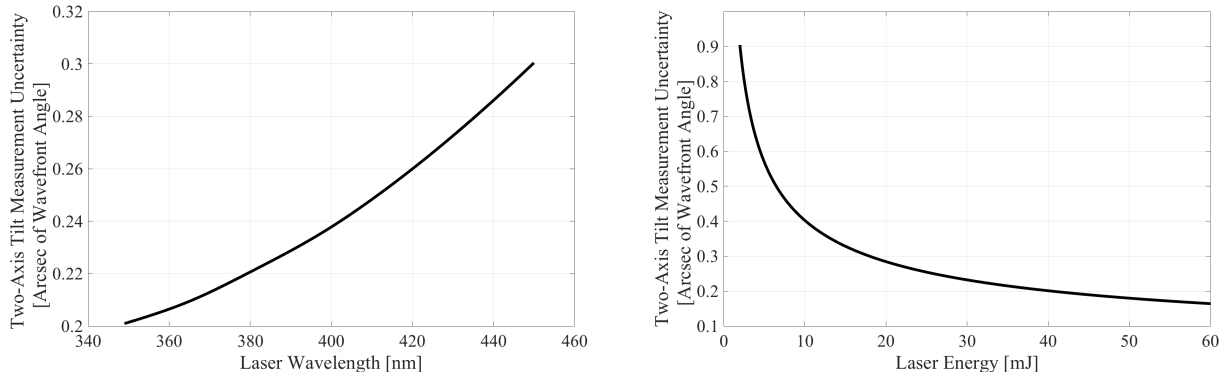


Figure 3. Left: For E of 40 mJ, $\sigma_{best,Las,1} = \sigma_{best,final}$ as a function of $\lambda_{1,1,1}$. Right: Using only the 349 nm laser (i.e. $\lambda_{1,1,1} = 349$ nm), $\sigma_{best,Las,1} = \sigma_{best,final}$ as function of E . Note that $f_p = 5$ kHz here.

The left plot in Figure 3 shows that taking into account the transmission of atmosphere¹⁰ and Raman cross section⁷ both as a function of wavelength, a shorter wavelength (the minimum being 349 nm in the plot) results in less uncertainty in the tilt measurement. The right plot in Figure 3 shows that even though saturation is not an issue in RRPLGS, shot noise limits the effectiveness of increasing laser power. Clearly, strategies other than maximizing the laser power are necessary to demonstrate the full potential of RRPLGS.

7. CONCLUSIONS AND ACKNOWLEDGEMENTS

Preliminary analysis and simulations have shown that RRPLGS is an approach worth investigating for object-independent tilt correction. Furthermore, as laser technology improves, RRPLGS will become more promising. One can imagine the concept of RRPLGS being applied with a high power next-generation supercontinuum laser yielding many combinations of two-axis tilt measurements for an improved measurement. A simulation using three lasers and only one Raman process has shown a combined two-axis tilt measurement uncertainty that is 1.2 times the diffraction limit.

RRPLGS allows for tip-tilt correction that is independent of natural guide stars and light from the object itself. Thus the applications of RRPLGS are wide-ranging. Even if only a partial correction is achieved, there are suitable applications such as wide-field ground-layer adaptive optics systems.

Future work includes using multiple returned wavelengths from various Raman scattering mechanisms to simulate a combination of tilt measurements in the context of a single laser. Adding to this the combination of measurements in the context of multiple lasers, the potential of RRPLGS can be further demonstrated. Also of interest is a more comprehensive system model, as well as building an RRPLGS prototype to acquire on-sky data and verify simulations.

The authors acknowledge and thank Matthew Kupinski for statistics guidance and Khanh Kieu for Raman scattering guidance, both of whom are faculty of the University of Arizona College of Optical Sciences.

REFERENCES

- [1] Foy, R., Migus, A., Biraben, F., Grynberg, G., McCullough, P. R., and Tallon, M., “The polychromatic artificial sodium star: a new concept for correcting the atmospheric tilt.,” **111**, 569 (Jun 1995).
- [2] Angel, R. and Lloyd-Hart, M., “Atmospheric tomography with Rayleigh laser beacons for correction of wide fields and 30-m-class telescopes,” in [*Astronomical Telescopes and Instrumentation*], (2000).
- [3] Hardy, J. W., [*Adaptive Optics for Astronomical Telescopes*], Oxford University Press, Oxford (1998).
- [4] Schöck, M., Foy, R., Tallon, M., Noethe, L., and Pique, J. P., “Performance analysis of polychromatic laser guide stars used for wavefront tilt sensing,” **337**, 910–920 (Dec 2002).
- [5] Thompson, L. A. and Gardner, C. S., “Excimer laser guide star techniques for adaptive imaging in astronomy,” in [*Active Telescope Systems*], Roddier, F. J., ed., **1114**, 184–190 (Sept. 1989).
- [6] Tyler, G. A., “Bandwidth considerations for tracking through turbulence,” *Journal of the Optical Society of America A* **11**, 358–367 (Jan. 1994).
- [7] Bischel, W. K. and Black, G., “Wavelength dependence of Raman scattering cross sections from 200-600 nm,” *AIP Conference Proceedings* **100**(1), 181–187 (1983).
- [8] Willitsford, A., *Resonance Raman Spectroscopy in the Ultraviolet using a Tunable Laser*, PhD thesis, Penn. State University (2008).
- [9] Penney, C. M., Peters, R. L. S., and Lapp, M., “Absolute rotational Raman cross sections for N₂, O₂, and CO₂,” *J. Opt. Soc. Am.* **64**, 712–716 (May 1974).
- [10] Valley, S., [*Handbook of Geophysics and Space Environments*], McGraw-Hill, New York (1965).
- [11] Allen, C. W., [*Astrophysical Quantities*], Athlone Press, London, 3rd ed. (1973).